# The physics of nanowire superconducting single-photon detectors

Renema, J.J.

# Chapter 1

# Introduction

## 1.1 Superconducting Single-Photon Detectors

Superconducting single-photon detectors [1] are an important technology for photodetection in the near infrared, with a wide range of applications. These detectors consist of a thin layer of superconducting material, which is nanofabricated into a wire. The typical wires which are used in applications are 4 nm thick, 100 nm wide and some tens of $\mu$m long, folded in a meander shape. Such photodetectors were first demonstrated at Moscow State Pedagogical University in 2001.

This type of photodetector has many practical advantages [2, 3]. Contrary to semiconductor-based single-photon detectors, the wavelength of photons which can be measured by the detector is not limited to the bandgap of the material but by the thickness and width of the wire, enabling detection of photons of up to 5 $\mu$m [4]. The electrical pulses corresponding to

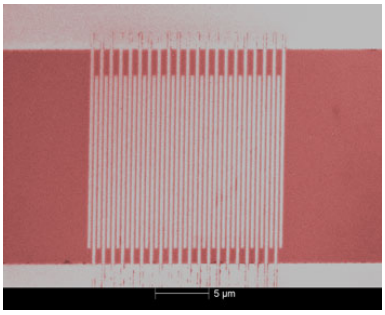


Figure 1.1: Scanning Electron Microscope image of a typical superconducting single-photon detector of the application-oriented meander type. Image courtesy of NIST.

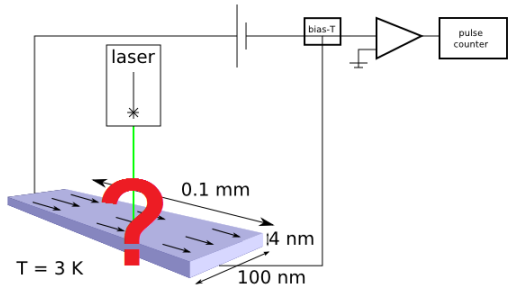


Figure 1.2: The central question of this thesis: what happens at the question mark?

a detection event have a rapidly rising flank with timing jitter in the 20-30 ps range [5], which enables accurate determination of the arrival time of the photon. These properties have many advantages in e.g. deep space communication applications, where bits are coded by the photon arrival time [6]. Moreover, these detectors have a very low dark count rate compared to avalanche photodiodes operating in the same wavelength range, and a fast reset time compared to transition edge sensors. The efficiency of such detectors can be enhanced strongly by embedding the detector inside a cavity [7].

These specifications make SSPDs excellent candidates for many technological and scientific applications. However, the detection mechanism is poorly understood. Though a considerable part of the working mechanism is well understood, much is still unclear about the central part of the detection process, where an absorbed photon is converted into a detection pulse [8].

The well-understood parts of the detection process are as follows: a photon is absorbed into the wire. This creates a cloud of quasiparticles, which obstructs the current flow, leading to a normal cross-section in the wire. This normal cross-section then grows under the influence of Joule heating, producing a voltage pulse [9]. The initial and final parts of this process are well understood: by solving Maxwell's equations for the appropriate geometry, we can investigate the absorption probability into the wire [10, 11, 12, 13]. We also understand the coupled electronic and heat diffusion equations which describe how the normal domain grows [9, 14].

The poorly understood step is how a single photon causes an obstruction across the wire. This thesis deals with that central step of the detection process, where an absorbed photon is converted into an excitation pulse. We investigate this problem by using a combination of three elements in our experiments: quantum detector tomography, multiphoton excitations and a nanodetector (our experimental sample).

The structure of this thesis is as follows: in this introductory chapter, I will set the stage by introducing the four main models of photodetection in superconducting single-photon detectors, as well the experimental techniques

used in this thesis. In Chapter 2, I will demonstrate quantum detector tomography, the main experimental method used throughout most of this thesis, which serves to accurately and completely characterize the response of an SSPD to incoming light pulses. In Chapter 3 and 4, I will apply this technique to investigate the physics of an SSPD. Chapter 3 presents results on SSPD physics which are preparatory for Chapter 4. In Chapter 4, we arrive at the central result of this thesis: we use quantum detector tomography to find which of the models of the detection event in SSPDs conforms to our experimental data.

The rest of the thesis is concerned with investigating various implications of this model. In Chapter 5, we combine experimental data and numerical simulations to investigate the position-dependence of the properties of the detection mechanism at the nanoscale level. Chapter 6 is somewhat separate from the rest of the thesis; in this chapter we investigate the effect of magnetic fields on the detection response. In Chapter 7, we investigate the size of an excitation in the detector using a two-photon technique.

This thesis is structured as a series of scientific papers, some of which have already been published. For articles already in press, we have aimed to keep as close to the original text as possible. In places where insights of earlier papers are expanded upon in later papers, we refer to the future work in footnotes.

## 1.2 Detector Physics of SSPDs

Discussion about the exact detection mechanism in SSPDs began soon after their invention [15]. Two key questions in the understanding of SSPDs are whether there is a role for a section of normal-state material in the detection event and whether magnetic vortices play a role. In this section, I will introduce the four models of the SSPD detection mechanism. A particularly crucial feature of these models is the *energy-current relation*, which describes the combinations of bias current and photon energy required to produce a detection event. The current required to obtain a detection event with a particular probability is called the threshold current $I_{th}$. Measurements of the energy-current relation are the primary method of investigation in SSPD detector physics. An excellent, more extended introduction to the various models is given in [16].

### 1.2.1 Normal-Core Hotspot Model

The earliest attempts to model the detection process in SSPDs focussed on the observation that the energy of the photon rapidly drops to below the level required to make any part of the wire normal after a photon absorption event. Therefore, this model focussed on a small, sharply defined, normal-state disruption of the wire, called a hotspot [1, 15] (see Figure 1.3 a). In

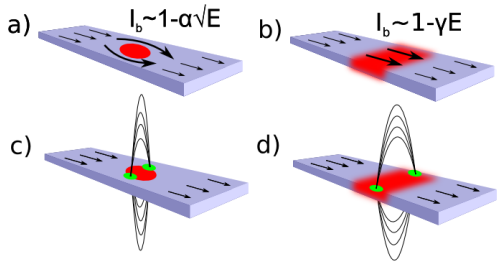


Figure 1.3: Schematic overview of the four main theories of the detection mechanism in SSPDs. (a) In the normal-core hotspot model, the photon energy creates a normal domain inside the superconductor, which the current has to bypass. (b) In the diffusion-based hotspot model, the quasiparticles diffuse outward from the point of absorption, creating a band of depleted superconductivity. (c) In the vortex nucleation model, a vortex-antivortex pair is formed in the hotspot. (d) In the vortex crossing model, either a vortex or a vortex-antivortex pair (pictured) uses an area of weakened superconductivity to cross the wire and annihilate. Picture is not to scale. From [17].

this model, the detection mechanism is as follows: after photon absorption, a normal hotspot forms, and the current is diverted around the hotspot. If the diameter of the hotspot is big enough, the critical current density will be exceeded in the cross-section containing the widest part of the hotspot and a detection event will occur through the suppression of superconductivity across the wire.

This model is essentially based on an area argument: each unit of energy contributes to making the hotspot larger, which serves to increase the diameter of the obstacle that the current must overcome. Since the system is 2D, the size scales as $\sqrt{E}$, and the energy-current relation is quadratic:

$$E = E_0(1 - I_{th}/I_c)^2, \tag{1.1}$$

where $E$ is the energy of the incident photon, $I_{th}$ is the threshold current, $I_c$ is the critical (depairing) current and $E_0$ is some energy scale.

### 1.2.2 Diffusion-Based Hotspot Model

A more sophisticated model was put forward in 2005 by Semenov *et al.* [18], who computed the number of Cooper pairs destroyed by the initial excitation and their subsequent spatial distribution due to diffusion and recombination (see Figure 1.3 b). In this model, there is no role for the normal state in a detection event. Instead, the number of Cooper pairs in a section of the wire with a length equal to the coherence length - called a $\xi$-slab - is

considered. These Cooper pairs, which are reduced in number compared to the unperturbed superconductor, must still carry the current which was carried by the original number of pairs. Therefore, they must speed up. If the Cooper pairs exceed the critical velocity $v_c$, they break up and the wire transitions to the normal state.

This model (also called the *refined hotspot model* in literature) consists essentially of counting Cooper pairs: the effect of the presence of quasiparticles on the energy gap is neglected, for example, and all Cooper pairs in the $\xi$-slab are equivalent. Since the current carrying capacity of the wire is proportional to the number of remaining Cooper pairs, the energy-current relation is therefore of the form:

$$E = E_0(1 - I_{th}/I_c), \tag{1.2}$$

with all quantities having the same interpretation as in equation 1.1. In this model, a precise computation of $E_0$ is possible, which was found to be [18]:

$$E_0 = (N_0\Delta^2 wd/\varsigma)\sqrt{\pi D\tau}, \tag{1.3}$$

where $N_0$ is the density of states at the Fermi level, $\Delta$ the superconducting energy gap, $w$ the width of the wire, $d$ the thickness, $D$ the diffusion coefficient of the material for quasiparticles and $\tau$ the timescale for quasiparticle multiplication. The dimensionless parameter $\varsigma$ represents the efficiency with which a photon is converted from an initial excitation in the material to quasiparticles at the superconducting band-edge. It captures, for example, losses to the phonon bath. Since the value of this parameter could in principle differ from film to film, it serves essentially as a fit parameter for each set of experimental observations.

This model achieved agreement with the experimental data on some aspects. In particular, the threshold currents computed with this model show reasonable agreement with experimental results. Moreover, equation 1.3 gives direction for experiments on the dependence of the detectable photon energy on various material parameters. However, this model still has limitations. In particular, the combined temperature dependence of equations 1.2 and 1.3 has the wrong sign [8]: if the temperature is increased, the main effect is the decrease of $\Delta$, which would imply a decrease of the energy which can be detected at a constant value of $I_b/I_c$. This has the interpretation that as the energy of each Cooper pair decreases, a photon of a given energy will break more of them, resulting in a more efficient detection process. However, the opposite trend (i.e. less efficient photodetection at higher temperatures) is consistently observed in experiments.

A further weakness of both the normal-core hotspot model and the diffusion-based hotspot model is that they both predict a deterministic, threshold-like response: the detector responds to all photons of a particular energy, or it doesn't. In contrast, experimentally (see Figure 1.4), it is observed that there is a slow roll-off when the bias current through the device

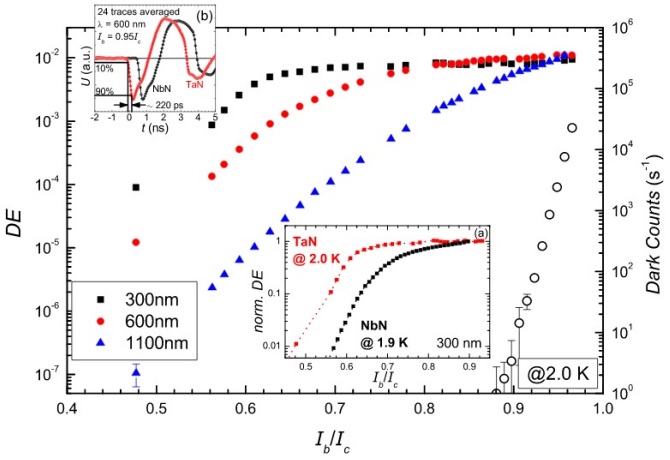


Figure 1.4: Typical count rate curves for an SSPD as a function of the applied bias current (taken from [20] of Engel *et al.*). The graph shows the detection efficiency of a TaN SSPD to three different wavelengths. At short wavelengths, the SSPD response consists of three regimes: a regime where the detection probability is exponential in the applied bias current, followed by an intermediate regime, and then a regime in which the detection probability is more or less independent of applied bias current. As the photon energy is decreased, the transition points between these regimes shift to higher bias current.

is decreased. This points to a regime in which some sort of fluctuation, either thermal or quantum mechanical in nature, occasionaly assists in producing a detection event. Magnetic vortices [19] are a natural candidate for this phenomenon. We first give an extremely succinct overview of the physics of vortices in thin films, before returning to the SSPD detection models which contain vortices.

### 1.2.3 Vortices

Vortices are structures that can occur within a type-II superconductor, i.e. one which has $\lambda > \xi/\sqrt{2}$ , with $\lambda$ the penetration length and $\xi$ the coherence length. These structures encompass a single magnetic flux quantum $\Phi_0$. They consist of a ring current, which if unobstructed extends over the penetration length $\lambda$, as well as a normal-state core, which has a size of the order of the coherence length $\xi$. Depending on the orientation of the ring current, one speaks of a vortex or an antivortex. Vortices have a magnetic interaction with their environment: vortices of equal orientation repel one another, whereas a vortex and an antivortex attract one another. A

vortex moving through a superconductor experiences friction and therefore dissipates energy into the wire.

For the present discussion, two forces which vortices can experience are relevant. First, vortices respond to the Lorentz force caused by an applied bias current. Second, in narrow wires, vortices experience an attractive force towards the edge of the wire. This is due to the fact that the ring current which surrounds the vortex cannot form without encountering the edge of the wire. In our system, the effective penetration length is different from the bulk value because $d \ll \lambda$, so we have $\Lambda_\perp = \lambda^2/d \approx 50$ $\mu$m, with $\lambda$ the bulk magnetic penetration length of 500 nm [21]. Since the width of the wire is typically 100-200 nm, this effect is prominent in our system.

We can find the forces resulting from this effect by considering the method of mirror charges from electrostatics. A charge above a grounded surface is attracted to that surface because of the induced charge on the surface, which we can model as the opposite charge at the point of the mirror image of the original charge. In the same way, we can represent the effects of the boundary conditions on a vortex in a thin wire by considering a mirror-antivortex outside the wire. In the case of a very thin wire, we must also consider the mirror-image of the mirror-image on the other side of the wire, and so on. Summing up all these forces results in an effective attractive force towards the edge of the wire, called an *edge barrier* [22].

### 1.2.4 Diffusion-Based Vortex Model

In 2008, Semenov *et al.* [23] put forward the notion that vortex-antivortex pairs (VAP) are responsible for the slow roll-off of the detection efficiency at longer wavelengths and lower currents. In 2011, Bulaevskii *et al.* suggested that vortices are responsible for all detection events, including those at high current (see Figure 1.3 d) [24, 25]. In this model, the arrival of the photon decreases the entry barrier for vortices, which enables a vortex crossing. Bulaevskii *et al.* also calculated the current which is required to have sufficient dissipation to cause a transition to the normal state; they showed that this current is much less than the typical operating currents of SSPDs. In this model, the functional dependence of the detection probability $R$ in the regime $R \ll 1$ is of the form [25]:

$$R \propto I_b^{\nu_h+1}, \tag{1.4}$$

where $\nu_h$ is a parameter that measures the reduction of the energy barrier for vortex entry to the absorption of a photon. Following [16, 25, 26], we apply the assumption that the energy is divided equally over the area of interest. This results in a value of $\nu_h$ of:

$$\nu_h = \nu - 4\pi\varsigma E/(k_b T)(\xi/w)^2, \tag{1.5}$$

where $\nu = \varepsilon_0/(k_bT)$ is the value in the absence of photon absorption, which was found to be 40-110 for dark counts [25] and 3-8 for photon counts [26], and $k_bT$ is the Boltzman energy. The two expressions above imply an energy-current relation of the form

$$I/I_0 = \exp(C/(\nu - E/E_0 + 1)), \tag{1.6}$$

with $C$ some constant. For comparison with the other models, this can be cast in an approximate form which is similar to the equations given above [27]:

$$E/E_0 = (1 - (I/I_c)^{4/3}). \tag{1.7}$$

A more advanced version of this model was producd by Engel and Schilling [28], who considered both the vortex physics described above and the diffusion of quasiparticles from the inital absorption spot. The complex nature of the model means that at this point, numerical simulations are the only way to obtain experimentally verifiable results. Engel and Schilling implemented a numerical simulation of quasiparticle diffusion and recombination, as well as current flow, and computed the entry energy for vortices. They showed that in this model, the energy-current relation is linear, i.e. follows equation 1.2. The fact that the energy-current relation depends on the shape of the quasiparticle cloud points - incidentally - to the importance which the quasiparticle distribution has for the detection mechanism.

One crucial difference between the diffusion-based vortex model and the two hotspot models is that the critical current in the vortex model is no longer the depairing current but the current at which vortices unbind from the edge of the wire. This current has a value of approximately $I_c \approx 0.8 I_{c,dep}$. Whereas the difference between these currents might seem like a natural way of testing which of the models is correct, unfortunately these two quantities have the same temperature dependence $I \propto 1/t^{3/2}$ [24, 25], with $t \equiv (1-T/T_c)$, with $T$ the temperature and $T_c$ the critical temperature, which precludes this route[1].

The first version of the diffusion-based vortex model [28] did not implement current continuity; at each cross-section of the device the current density was simply assumed to be locally proportional to the number of available Cooper pairs, normalized in such a way as to have the same current in each cross-section of the device. That is: the current was assumed to go where the Cooper pairs were, which amounts to neglecting the terms in $\partial j/\partial x$, where $x$ is the coordinate along the cross-section of the wire. However, current crowding [29], i.e. the effect that even in a homogeneous wire, the current flows around obstacles in a non-homogeneous way, was known to be a significant effect in SSPDs [30, 31]. Implementing full current continuity as well as suppression of the superconductivity due to the presence

[1] Using the Ginzburg-Landau temperature dependence

of a bias current leads to a more complete set of predictions [32], which will be the subject of Chapter 5 of this thesis.

### 1.2.5 Normal-State Vortex Model

A fourth model was formulated by Zotova and Vodolazov [33] (see Figure 1.3 c), who approached the problem in the context of the time-dependent Ginzburg-Landau equation. The starting point of this study was a normal-core hotspot, around which a vortex antivortex pair forms, which are then driven to the edges of the wire, causing a transition to the normal state in a manner similar to the diffusion-based scenario.

This model was revised several times. In the initial version of this model, the energy-current relation was almost equivalent to that of the normal-state hotspot model. Later [16], a correction term was added which takes into account the fact that the superconductivity inside the hotspot is not entirely surpressed. This produces deviations from the normal-core relation, which flatten the energy-current relation, bringing the model more in line with experimental results. After this, further corrections [34, 35] were added which pertain to the proximity effect induced by the normal-state region into the surrounding superconducting material. With these corrections, the normal-state vortex model predicts an almost linear energy-current relation in the regime which has been accessible to experiments so far.

The normal-state vortex model and the diffusion-based vortex model differ in three crucial aspects. First, in the diffusion-based model, vortices always enter the wire via the sides. In the normal-state model, in constrast, vortices can also enter from the edges of the normal-state hotspot, and it is predicted that for some cases, this is the energetically more favorable route. Secondly in the normal-state vortex model, the critical current of the wire is the depairing current. This means that the energy-current relation contains a strongly nonlinear part at photon energies of the order of a hundred meV, i.e. in the mid-infrared. Neither of these predictions has yet been subjected to experiment [16].

Third, the two models differ in their predictions on the influence of a magnetic field on the detection efficiency. In the diffusion-based model this dependence is strong, since vortices enter from the sides of the wire, where the current is most affected by the applied field. In the normal-state vortex model, in contrast, this dependence is weak, especially at high detection probabilities, since for most detection events the vortices nucleate near the center of the wire, where the current density is not affected by the applied field.

However, since both models contain essentially similar physics, approached in two different theoretical frameworks, it is conceivable that the two models will eventually both be refined to the point where they produce the same results.

### 1.2.6 Other Features of the Detection Process

In the meantime, other aspects of the detection mechanism were elucidated. The electro-thermal mechanism by which the detector resets after a detection event was investigated by Kerman *et al.* [9], who pointed out the role of kinetic inductance in the modelling of the eletrical properties of this system. In a seminal work by Clem and Berggren [29], current crowding in the bends of the meander was identified as the major limitation on the critical current [31] in meander-type detectors. The photo-absorption into the wire was also investigated. It was demonstrated that the detector is polarization-sensitive: the electric field parallel to the wires is absorbed preferentially compared to field perpendicular to the wires [10, 11, 12, 13].

## 1.3 Experimental Techniques

In this section, I will introduce the three main features of our experiment: quantum detector tomography, multiphoton detection and the nanodetector.

### 1.3.1 Quantum Detector Tomography

Quantum detector tomography is an experimental procedure to measure the detection statistics of a photodetector whose response is unknown[2]. The goal is to find the response of the detector in the number state (Fock) basis, i.e. to find out what would happen if the detector were to receive exactly $n$ photons as an input. This experiment was first demonstated by Lundeen *et al.* [36, 37], who performed detector tomography on an avalanche photodiode.

It would be most straightforward to probe the detection statistics directly in the Fock basis, but these states are not easily experimentally available. Therefore, it is much easier to use states which are some superposition in the number state basis, which are produced by conventional light sources. Since the detector is not sensitive to the phase of the incoming photon, we may adopt a classical picture in which we consider only the photon number probability distribution, i.e. we restrict ourselves to the diagonal elements of the density matrix. The strategy is then to measure the detection probability for many different photon number probability distributions, and apply a transformation to convert these results into the response in the number state basis.

The most convenient set of states to use for quantum detector tomography is the set of coherent states. These states, which are produced by a laser, have the convenient property that an attenuated coherent state still remains coherent. This means that it is possible to create the desired set of photon number probability distributions simply by attenuation.

[2]The quantum detector tomography code used throughout this thesis is available on request from the author.

The experiment is then to take a pulsed laser with a well-defined pulse energy and apply fixed attenuation and measure the detection probability. If we have sufficient statistics for this attenuation, we go to the next attenuation, and so on. By repeating this process for sufficiently many attenuations it becomes possible to find the response of the detector in the Fock basis.

It should be noted that the transformation that converts the experimental results into a description in the number state basis is not necessarily simple. The transformation can strongly amplify measurement noise, or even produce nonphysical results. In fact, a branch of mathematics is dedicated precisely to finding convenient transformations for various types of problems of this nature [38]. The usual strategy is to restrict the transformation on the basis of some additional information which was not previously considered. In the case of quantum detector tomography, this is usually done by assuming that the response to different numbers of photons doesn't change strongly for adjacent photon numbers, i.e. if we know the detection probability of $n$ photons $p_n$, then our zeroth-order guess for $p_{n+1} \approx p_n$. This restriction can by applied in various mathematical guises, and turns out to be sufficient to 'tame' the transformation.

### 1.3.2 Multiphoton Detection

Multiphoton detection refers to the phenomenon that two photons absorbed simultaneously in the detector can lead to a detection event. These detection events occur at lower currents than single-photon detection events, even when a single photon does not. This effect was noticed early on in the development of SSPDs [1] (see Figure 1.5), but didn't find any applications until Bitauld *et al.* [39] showed multiphoton nanoscale imaging and Zhou *et al.* [40] showed that this effect could be used to build an ultrasensitive higher-order autocorrelator.

We use multiphoton detection as a tool for probing the detection mechanism. Multiphoton detection has two strong advantages compared to single-photon detection when it comes to experiments into the physics of the detection mechanism.

The first advantage is that it enables the experimenter to excite the detector with a range of energies in a single experiment, at a single wavelength. This means that the relation between bias current and photon energy can be measured in a single experimental configuration, without changing the wavelength of the incident light. Changing the wavelength of the incident light usually means changing the intensity, and the size of the illumination spot, leading to different illumination conditions [16]. Using multiphoton excitation sidesteps this problem.

The second advantage is that multiphoton excitation allows for a much larger range of photon energies to be used than in single-photon excitation. Typically, a source is only tunable in a particular wavelength range, and this dynamic range can be hugely extended by using multiphoton excitations.

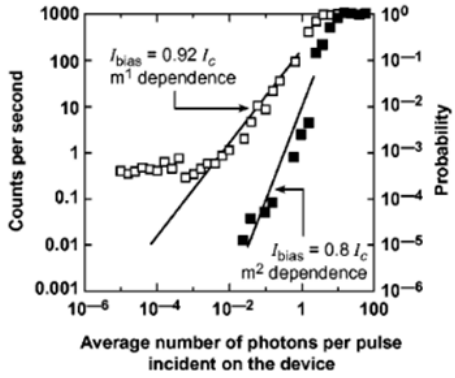


Figure 1.5: The earliest measurement on two-photon processes in SSPDs. The solid black squares represent the detector operating in a two-photon mode, which occurs at lower bias current. The quadratic dependence of the count rate on the input photon number is a signature of a two-photon process. From [1].

Also, the sample substrate, the windows of the cryostat, or even the air of the laboratory may all be absorbing at particular energies of interest. Using multiphoton excitations solves this issue.

### 1.3.3 Nanodetector

The nanodetector is a particular geometry for SSPDs (see Figure 1.6), first developed by Bitault *et al.* [39], which is convenient for experiments on SSPD physics. In this geometry, the usual meander is reduced to a single line contact between two tapered banks. In a variant of this design, there is a short (a few hundred nm) bridge between the two banks. Only the central part of this device (the line contact or the bridge) is photodetecting, the banks merely serve as contact points for the bias current. An inductor which serves to balance the reset time of the detector with its cooling time is connected in series to the detector, to prevent latching [9].

For fundamental studies, this geometry has three main advantages: robustness, simplicity and enhanced multiphoton response. First, this geometry is less sensitive to fabrication errors. It is difficult to make a long wire with uniform edges. Any notch, bulge or other imperfection in the wire (the phenomenological term for such imperfections is *constrictions* [41]) will be more strongly photodetecting than the rest of the wire, leading to experimental results which are difficult to interpret.

Secondly, the nanodetector doesn't contain any bends. In previous experiments, indications were found that bends behave differently than straight sections of wire [26, 42]. Normally, samples are considered which contain

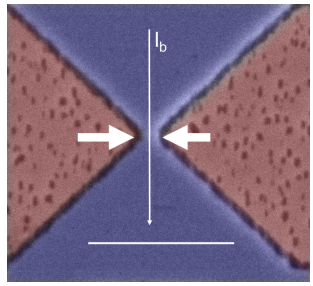


Figure 1.6: False-colour SEM image of our detector. The blue area indicates the NbN layer, the red areas indicate places where the layer has been etched away. The two thick arrows indicate the active part of the detector. The vertical arrow indicates the direction of the current flow. The horizontal while line is a 1 $\mu$m scale bar. Image courtesy of Döndü Sahin.

both bends and straight sections. It can be unclear whether photodetection results from the bends or not. Moreover, for phenomena such as the critical current of an SSPD, the bends are the dominant feature [31], obscuring the intrinsic response of the wire.

A third advantage of a nanodetector is that it has a relatively enhanced multiphoton response. In a meander geometry, it is necessary for two photons to be absorbed within some distance from each other in order to trigger a two-photon detection event [43, 44]. However, each photon individually will also have a finite, but strongly reduced possibility of triggering the detector. For a sufficiently long wire, however, this effect will dominate over the two-photon effect. In a more compact geometry, all absorbed photons contribute to photodetection. This is therefore a suitable geometry in which to study multiphoton detection events.